Key phosphorylation sites in GPCRs orchestrate the contribution of β-Arrestin 1 in ERK1/2 activation

Mithu Baidya[1,†], Punita Kumari[1,†] (iD), Hemlata Dwivedi-Agnihotri[1,†], Shubhi Pandey[1] (iD), Madhu Chaturvedi[1], Tomasz Maciej Stepniewski[2,3], Kouki Kawakami[4], Yubo Cao[5], Stéphane A Laporte[5,6], Jana Selent[2], Asuka Inoue[4] & Arun K Shukla[1,*] (iD)

Abstract

β-arrestins (βarrs) are key regulators of G protein-coupled receptor (GPCR) signaling and trafficking, and their knockdown typically leads to a decrease in agonist-induced ERK1/2 MAP kinase activation. Interestingly, for some GPCRs, knockdown of βarr1 augments agonist-induced ERK1/2 phosphorylation although a mechanistic basis for this intriguing phenomenon is unclear. Here, we use selected GPCRs to explore a possible correlation between the spatial positioning of receptor phosphorylation sites and the contribution of βarr1 in ERK1/2 activation. We discover that engineering a spatially positioned double-phosphorylation-site cluster in the bradykinin receptor (B_2R), analogous to that present in the vasopressin receptor (V_2R), reverses the contribution of βarr1 in ERK1/2 activation from inhibitory to promotive. An intrabody sensor suggests a conformational mechanism for this role reversal of βarr1, and molecular dynamics simulation reveals a bifurcated salt bridge between this double-phosphorylation site cluster and Lys[294] in the lariat loop of βarr1, which directs the orientation of the lariat loop. Our findings provide novel insights into the opposite roles of βarr1 in ERK1/2 activation for different GPCRs with a direct relevance to biased agonism and novel therapeutics.

See also: **RT Premont** (September 2020)

Introduction

G protein-coupled receptors (GPCRs) recognize a diverse array of ligands but exhibit broadly conserved patterns of transducer coupling and regulatory paradigms (Bockaert & Pin, 1999). For example, agonist-induced receptor phosphorylation promotes coupling of multifunctional proteins called β-arrestins (βarrs), which are critically involved in the regulation of GPCR signaling and trafficking patterns (Freedman & Lefkowitz, 1996; Lefkowitz & Shenoy, 2005; DeWire *et al*, 2007). The ability of βarrs to mediate downstream signaling cascades has yielded new paradigms of GPCR signaling and led to the conceptual framework of biased agonism (Azzi *et al*, 2003; Wei *et al*, 2003; Shukla *et al*, 2011; Reiter *et al*, 2012). G protein and βarr bias has been described for a number of GPCRs, and in many cases, distinct functional profiles of these two pathways in terms of cellular and physiological outcomes have also been established (Luttrell & Gesty-Palmer, 2010; Appleton & Luttrell, 2013; Gesty-Palmer *et al*, 2013; Peterson & Luttrell, 2017). Although βarrs' contributions are documented in a number of downstream signaling pathways across different GPCRs, agonist-induced ERK1/2 MAP kinase phosphorylation has been one of the most common readout to probe βarr signaling profile and biased agonism (Azzi *et al*, 2003; Wei *et al*, 2003; Lefkowitz & Shenoy, 2005; DeWire *et al*, 2007).

βarrs are typically observed to contribute positively in ERK1/2 MAP kinase phosphorylation and activation; however, in some cases, the two isoforms, namely βarr1 and 2, play opposite roles (DeWire *et al*, 2007; Srivastava *et al*, 2015). For example, depletion of βarr1 results in an increase in ERK1/2 phosphorylation while reducing the levels of βarr2 leads to significant decrease for several GPCRs including the angiotensin receptor ($AT_{1a}R$) and bradykinin receptor (B_2R; Ahn *et al*, 2004; Zimmerman *et al*, 2011). A mechanistic understanding for this intriguing functional diversity between the two βarr isoforms is currently lacking, and it represents a missing link in our understanding of GPCR-βarr signaling system.

1 Department of Biological Sciences and Bioengineering, Indian Institute of Technology, Kanpur, India
2 Research Programme on Biomedical Informatics (GRIB), Department of Experimental and Health Sciences of Pompeu, Fabra University (UPF)-Hospital del Mar Medical Research Institute (IMIM), Barcelona, Spain
3 Faculty of Chemistry, Biological and Chemical Research Centre, University of Warsaw, Warsaw, Poland
4 Graduate School of Pharmaceutical Sciences, Tohoku University, Sendai, Japan
5 Department of Pharmacology and Therapeutics, McGill University, Montréal, QC, Canada
6 Department of Medicine, McGill University Health Center, McGill University, Montréal, QC, Canada
*Corresponding author. Tel: +91-512-679-4251; E-mail: arshukla@iitk.ac.in
†These authors contributed equally to this work

Therefore, understanding the details of βarrs' contribution in ERK1/2 activation, especially the diversity across different receptor systems, requires additional studies.

Receptor phosphorylation is a key determinant of the interaction between βarrs and GPCRs, and it is well established that differential phosphorylation patterns on the receptor can fine-tune βarr conformation and ensuing functional outcomes (Gurevich & Gurevich, 2004, 2018b; Reiter & Lefkowitz, 2006; Ranjan *et al*, 2017; Chen *et al*, 2018). For example, receptor phosphorylation by different GRKs results in distinct phosphorylation patterns, which in turn guide different conformations in recruited βarrs and functional outcomes, a framework referred to as the "bar code" mechanism (Kim *et al*, 2005; Ren *et al*, 2005; Shukla *et al*, 2008). More recently, a "phosphorylation code"-based mechanism has been proposed for GPCR-βarr interaction based on the crystal structure of rhodopsin–arrestin complex (Zhou *et al*, 2017). Considering the three conserved positively charged pockets on the N-domain of arrestin, the requirement of at least three phosphorylated residues in GPCRs, which are separated by additional residues forming a spatial pattern, was conceived for high-affinity interaction between the receptor and arrestin in this study (Zhou *et al*, 2017). This spatial arrangement of phosphorylation sites on GPCRs was referred to as "phosphorylation code" with two different patterns, i.e., PxPxxP/E/D (short code) and PxxPxxP/E/D (long code), where P refers to a phospho-Ser or phospho-Thr and X refers to any other amino acid except proline (Zhou *et al*, 2017). While the contribution of these phosphorylation patterns in arrestin recruitment was experimentally measured for rhodopsin and β2 adrenergic receptor, a direct correlation between such phosphorylation patterns and βarr-mediated signaling, if any, was not investigated (Zhou *et al*, 2017).

Here, we set out to probe the contribution of spatial positioning and pattern of phosphorylation sites in selected GPCRs in determining the role of βarr1 in ERK1/2 phosphorylation. We discover that certain key positions, in the context of phosphorylation site clusters, orchestrate the differential contribution of βarr1 in agonist-induced ERK1/2 activation for different GPCRs. An intrabody sensor suggests a conformational mechanism for this interesting phenomenon, which is further corroborated by molecular dynamics (MD) simulation. Our data offer mechanistic insights into distinct role of βarr1 in the activation of ERK1/2 MAP kinase downstream of different GPCRs, and it has direct implications for the novel paradigms of GPCR signaling and biased agonism.

Results

Receptor-specific contribution of βarr1 in ERK1/2 MAP kinase activation

In order to investigate the opposite contribution of βarr1 in agonist-induced ERK1/2 phosphorylation, and to link it with specific receptor phosphorylation sites, we first chose the V_2R and B_2R as model systems. Both of these receptors were originally categorized as "class B" GPCRs in terms of βarr recruitment and trafficking patterns (Oakley *et al*, 2000). That is, they interact with βarrs in a stable fashion and prolonged exposure with agonist results in their endocytotic trafficking together with βarrs. A subsequent study however differentiated B_2R from other class B GPCRs including V_2R,

by reporting that βarrs rapidly dissociate from this receptor in endosomes followed by receptor recycling to the plasma membrane (Simaan *et al*, 2005). The most interesting aspect that prompted us to choose these two receptor systems is that previous studies have demonstrated strikingly different contribution of βarr1 in agonist-induced ERK1/2 phosphorylation for these two receptors (Ren *et al*, 2005; Charest *et al*, 2007; Zimmerman *et al*, 2011; Oligny-Longpre *et al*, 2012; Ghosh *et al*, 2019). While βarr1 knockdown leads to a significant reduction in ERK1/2 phosphorylation downstream of V_2R (Ghosh *et al*, 2019), it results in an enhanced level of ERK1/2 phosphorylation for the B_2R (Zimmerman *et al*, 2011). In other words, βarr1 exerts a supportive role in ERK1/2 phosphorylation for the V_2R but an inhibitory role for the B_2R.

We first analyzed the potential phosphorylation site patterns in the carboxyl-terminus of these two receptors with reference to a recent study that has proposed "phosphorylation codes"-based mechanism of GPCR-βarr interaction (Zhou *et al*, 2017). This study suggested that spatial distribution of potential phosphorylation sites on the receptor is separated by additional residues to constitute PXPXXP and PXXPXXP type patterns, where P is pSer/pThr and X is any other amino acid (Zhou *et al*, 2017). We observed that both of these receptors (i.e., V_2R and B_2R) harbor two such phosphorylation site patterns in their carboxyl-terminus, i.e., ^{357}SCTTAS^{362} (i.e., PXPXXP) and ^{357}SCTTA SS^{363} (i.e., PXXPXXP) in V_2R and ^{366}SMGTLRT^{372} (i.e., PXXPXXP) and ^{369}TLRTSIS^{375} (PXXPXXP) in B_2R (Fig 1A). We also confirmed similar recruitment and trafficking patterns of βarr1 for V_2R and B_2R in HEK-293 cells by confocal microscopy and observed that agonist stimulation leads to surface localization of βarr1-mCherry first (2–5 min), followed by endosomal trafficking upon prolonged exposure (15–30 min; Fig 1B).

Next, we measured agonist-induced ERK1/2 phosphorylation downstream of V_2R and B_2R in HEK-293 cells under control and βarr1 knockdown conditions. In agreement with previous studies, we also observed that knockdown of βarr1 yielded a significant reduction in ERK1/2 phosphorylation for V_2R while it augmented the levels of ERK1/2 phosphorylation in the case of B_2R (Fig 1C and D). This striking difference between the V_2R and B_2R suggests that the mechanistic basis of βarr1 contribution in agonist-induced ERK1/2 activation is determined at levels other than their trafficking patterns and the number of phosphorylation site patterns.

Engineering a double-threonine cluster in B_2R reverses the contribution of βarr1

A comparison of the carboxyl-terminus sequences of the V_2R and B_2R revealed key differences in the spatial distribution of the potential phosphorylation sites (Fig 2A). While V_2R has "PXXPXXP" and "PXPXXP" type phospho-site patterns (where P is Ser/Thr and X is any residues including Ser/Thr), both the phospho-site patterns present in the B_2R are of "PXXPXXP" type (Fig 2A). This prompted us to generate a set of B_2R mutants that resemble the spatial pattern of phosphorylation sites in V_2R and test the contribution of βarr1 in ERK1/2 activation upon their activation (Fig 2B). These mutants expressed at comparable levels to B_2R^{WT} in HEK-293 cells (Fig EV1A), and the surface expression of the individual mutants between the control and βarr1 knockdown conditions were also comparable (Fig EV1B and C). These mutants also displayed typical "class B" pattern of βarr1 trafficking as assessed by confocal microscopy, similar to B_2R^{WT} (Fig 2C).
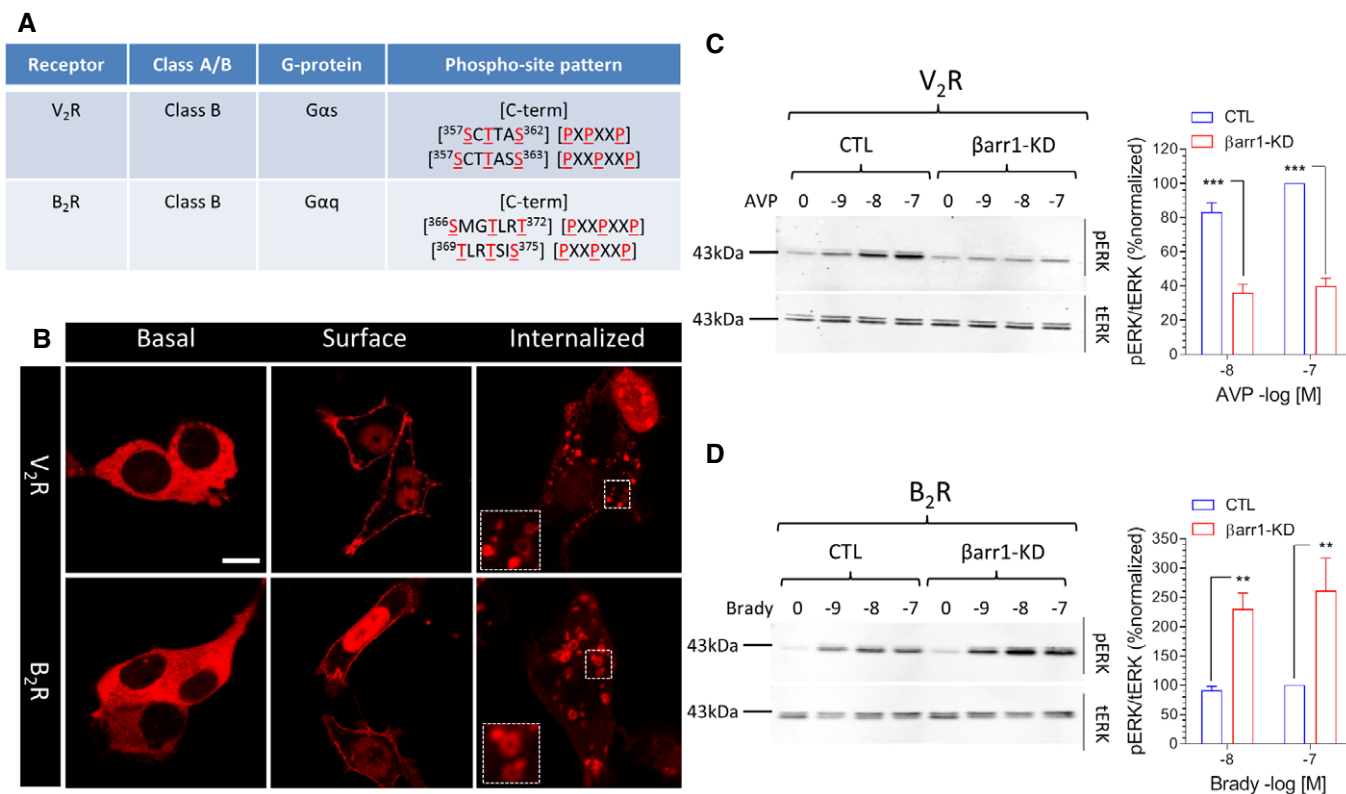
Figure 1. βarr1 has opposite contributions in agonist-induced ERK1/2 activation for V₂R and B₂R.

A   G-protein-coupling preference and phospho-site patterns in the carboxyl-terminus of V_2R and B_2R, deduced based on a previous study (Zhou et al, 2017). The phospho-site patterns in the form of PXPXXP and PXXPXXP are underlined and color-coded. Both V_2R and B_2R recruit βarrs in "class B" pattern (Oakley et al, 2000) as reflected by stable interaction and endosomal trafficking of the receptor-βarr complexes.

B   Confocal microscopy reveals typical "class B" pattern of βarr1 recruitment for V_2R and B_2R as reflected by first the localization at the plasma membrane and subsequently, internalization in endosomal vesicles upon agonist stimulation. HEK-293 cells expressing V_2R/B_2R and βarr1-mCherry were stimulated with agonist (AVP; 100 nM and Bradykinin; 100 nM), and the localization of βarr1 was visualized using confocal microscopy. Representative images from three independent experiments are shown here, and the scale bar is 10 μm. Visual scoring of images from three independent experiments revealed agonist-induced βarr1 recruitment (i.e., membrane and endosomal localization) in approximately 77% of the cells for V_2R (221 cells) and 75% of the cells for B_2R (662 cells).

C, D   Agonist-induced phosphorylation of ERK1/2 in HEK-293 cells expressing either V_2R or B_2R in the absence (control; CTL) and presence of βarr1 knockdown (βarr1-KD) are measured using Western blotting. Densitometry-based quantification of data (mean ± SEM) from four independent experiments is presented as bar graphs in the right panels, normalized with respect to maximal dose under control condition (treated as 100%), and analyzed using two-way ANOVA with Bonferroni multiple comparisons test (***$P < 0.001$, **$P < 0.01$).

Moreover, we also observed that these mutants are capable of robustly recruiting βarr1, similar to B_2R^{WT}, as measured using a NanoBiT assay (Dixon et al, 2016; Shihoya et al, 2018), although $B_2R^{\Delta I374}$ exhibits slightly lower level of βarr1 interaction (Fig 2D).

Among these mutants, the deletion of Gly^{368}, i.e., $B_2R^{\Delta G368}$, changes the phosphorylation site pattern from PXXPXXP pattern to PXPXXP. Still however, the inhibitory contribution of βarr1 in ERK1/2 activation remains unchanged, i.e., knockdown of βarr1 augments agonist-induced ERK1/2 phosphorylation, similar to that of B_2R^{WT} (Fig 3A). Strikingly, either the mutation of Leu^{370} alone, i.e., B_2R^{L370T}, or in combination with Gly^{368} deletion, i.e., $B_2R^{\Delta G368/L370T}$, reverses the contribution of βarr1 in ERK1/2 activation from inhibitory to supportive, and we observe a significant reduction in ERK1/2 phosphorylation upon βarr1 knockdown (Fig 3B and C). It is interesting to note that the PXXPXXP pattern is not altered in B_2R^{L370T} and $B_2R^{\Delta G368/L370T}$ mutants. Similar to $B_2R^{\Delta G368}$, the deletion of Ile^{374}, i.e., $B_2R^{\Delta I374}$, which disrupts the second PXXPXXP pattern, also does not affect the inhibitory contribution of βarr1 in

agonist-induced ERK1/2 phosphorylation (Fig 3D). These experiments presented in Fig 3 were carried out in HEK-293 cells where βarr1 was knocked down using stable expression of shRNA against βarr1. We also corroborated the role reversal of βarr1 in ERK1/2 phosphorylation for the selected B_2R mutants (B_2R^{L370T} and $B_2R^{L370T/\Delta G368}$) using CRISPR/Cas9 edited HEK-293 cells expressing either both βarrs or only βarr2 (Fig EV2). We observed a pattern of ERK1/2 phosphorylation (Fig EV2), which is very similar to that measured with shRNA approach (Fig 3).

The carboxyl-terminus sequence of V_2R contains two clusters of potential phosphorylation sites, which are T^{359}/T^{360} and $S^{362}/S^{363}/S^{364}$, and the B_2R lacks analogous clusters in its carboxyl-terminus (Fig 2A). A closer look at the potential phosphorylation sites in B_2R mutants, where βarr1 knockdown augments ERK1/2 activation (i.e., B_2R^{L370T} and $B_2R^{L370T/\Delta G368}$), suggests that these mutations construct a double-Threonine cluster (i.e., Thr^{369} and Thr^{370}), although they do not alter the PXXPXXP pattern. The $B_2R^{\Delta G368}$ mutant, which mimics the spatial distribution of Ser^{366} and Thr^{369}
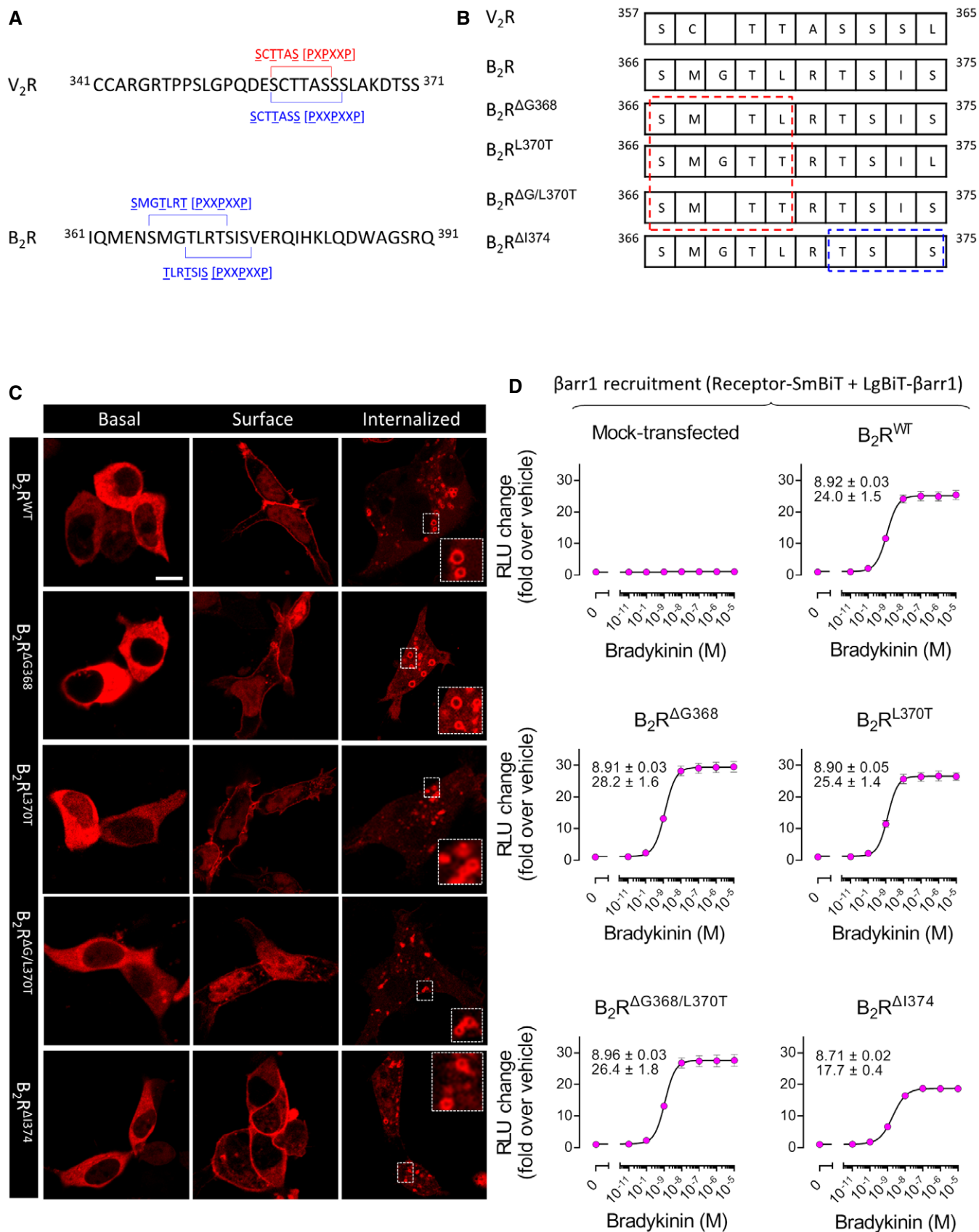
Figure 2.

Figure 2. Spatial distribution of phospho-sites and βarr1 recruitment of B$_2$R mutants.

A   Phospho-site clusters in the carboxyl-terminus of V$_2$R and B$_2$R are underlined and color-coded to reflect the PXPXXP and PXXPXXP patterns as proposed in a previous study (Zhou *et al*, 2017).

B   A number of B$_2$R mutants were generated to mimic the spatial distribution of phospho-site pattern of Ser/Thr as present in the V$_2$R. The first three mutants were designed to target the proximal part of the phospho-site pattern (indicated in red dotted box) while the fourth mutant was designed to target the distal part (indicated in blue dotted box).

C   Confocal microscopy reveals robust recruitment of βarr1 to B$_2$R mutant constructs upon agonist stimulation. HEK-293 cells expressing either B$_2$R^{WT} or B$_2$R mutants along with βarr1-mCherry were stimulated with agonist (Bradykinin; 100 nM), and the localization of βarr1 was visualized using confocal microscopy. Representative images from three independent experiments are shown here, and the scale bar is 10 µm. Visual scoring from three independent experiments revealed agonist-induced βarr1 recruitment (i.e., membrane and endosomal localization) in approximately 75% of the cells for B$_2$R^{WT} (662 cells), 74% of the cells for B$_2$R$^{\Delta G368}$ (169 cells), 75% of the cells for B$_2$R^{L370T} (130 cells), 85% of the cells for B$_2$R$^{\Delta G368/L370T}$ (132 cells), and 77% of the cells for B$_2$R$^{\Delta I374}$ (116 cells).

D   HEK-293 cells expressing B$_2$R constructs with C-terminal SmBiT and βarr1 with N-terminal LgBiT were treated with indicated concentrations of bradykinin, and ligand-induced change in luminescent signal was measured. Concentration-response curves were plotted using GraphPad Prism, and pEC$_{50}$ (top) and E$_{max}$ (bottom) were calculated. Data represent mean ± SEM of five independent experiments (three for B$_2$R$^{\Delta I374}$), each performed in duplicate.

in B$_2$R with that of Ser^{357} and Thr^{359} in V$_2$R, and the B$_2$R$^{\Delta I374}$ mutant, which constructs a triple phospho-site cluster in B$_2$R (Thr^{372}/Ser^{373}/Ser^{375}), similar to that in V$_2$R (Ser^{362}/Ser^{363}/Ser^{364}), retain the inhibitory contribution of βarr1 in ERK1/2 phosphorylation. Taken together, these data indicate that the presence of Leu^{370} in B$_2$R plays a critical role in the inhibitory contribution of βarr1 in ERK1/2 activation, and spatial positioning of a threonine in its place, which constructs a double-Thr cluster, reverses the contribution of βarr1.

Intrabody sensor reveals a conformational mechanism for the contribution of βarr1

In order to gain additional mechanistic insight into differential contribution of βarr1 in ERK1/2 activation for V$_2$R and B$_2$R, we used a previously described intrabody-based sensor of βarr1 conformation in cellular context (Ghosh *et al*, 2019; Baidya *et al*, 2020). This sensor is based on a synthetic antibody fragment referred to as Fab30 that selectively recognizes V$_2$R-bound βarr1 conformation *in vitro* (Shukla *et al*, 2013, 2014; Kumari *et al*, 2016, 2017; Ghosh *et al*, 2019). Moreover, an intrabody version of Fab30, referred to as Ib30, also recognizes βarr1 upon agonist stimulation of V$_2$R in cellular context (Ghosh *et al*, 2019). Recently, a YFP-tagged version of Ib30 has also been generated and used as a conformational probe for measuring the interaction and trafficking of βarr1 in cells upon GPCR stimulation (Baidya *et al*, 2020). As previously reported, we observed that Ib30-YFP efficiently recognizes V$_2$R-bound βarr1 and follows the trafficking pattern of βarr1 upon agonist stimulation (Figs 4A and EV3), but fails to recognize βarr1 upon stimulation of B$_2$R (Figs 4B and EV3). Inferring a potential conformational difference in βarr1 upon interaction with V$_2$R vs. B$_2$R, which may be correlated to its opposite contribution in ERK1/2 activation, we measured the ability of Ib30-YFP to recognize βarr1 in the context of B$_2$R mutants. Strikingly, we found robust reactivity of Ib30-YFP to βarr1 in the case of B$_2$R^{L370T} and B$_2$R$^{L370T/\Delta G368}$ mutants (Fig 4C and D), and it displayed a trafficking profile very similar to that observed of

V$_2$R. On the other hand, we observed only a weak reactivity of Ib30-YFP for the other two B$_2$R mutants (B$_2$R$^{\Delta G368}$ and B$_2$R$^{\Delta I374}$) where βarr1 plays an inhibitory role in ERK1/2 activation, similar to B$_2$R^{WT} (Fig EV4).

To further confirm these findings and measure the reactivity of Ib30 sensor more quantitatively, we designed a NanoBiT construct of Ib30 with N-terminal fusion of LgBiT. We then measured agonist-induced luminescence signal in HEK-293 cells expressing various B$_2$R constructs together with SmBiT-βarr1 and LgBiT-Ib30. We observed a pattern that is reminiscent of confocal microscopy data, i.e., Ib30 robustly recognizes V$_2$R^{WT} but does not recognize βarr1 for B$_2$R^{WT} (Fig 5A). Moreover, we also observed that Ib30 NanoBiT sensor does not recognize βarr1 for B$_2$R$^{\Delta G368}$ and only weakly recognizes βarr1 for B$_2$R$^{\Delta I374}$ (Fig 5A). However, Ib30-NanoBiT sensor exhibits significant interaction with βarr1 for B$_2$R^{L370T} and B$_2$R$^{\Delta G368/L370T}$ (Fig 5A), which is in excellent agreement with the pattern observed by confocal microscopy. Taken together, these findings suggest that spatial signature of receptor phosphorylation sites play a key role in ensuing βarr1 conformation recognizable by Ib30 and, thereby, potentially link βarr1 conformation with its contribution in ERK1/2 activation.

In order to confirm that the mutation of the receptor phosphorylation sites do not alter their G-protein coupling, we also measured agonist-induced activation of Gq heterotrimer for B$_2$R mutants using a previously described NanoBiT-G-protein dissociation assay (Inoue *et al*, 2019). As presented in Fig 5B, we observe that B$_2$R mutants exhibit G-protein activation profile similar to the wild-type receptor.

Structural insights into receptor-specific βarr1 conformations

In order to gain structural insights into these findings, we employed a molecular dynamics (MD) simulation approach using the previously determined crystal structure of βarr1 in the presence of V$_2$R phosphopeptide (V$_2$Rpp; Shukla *et al*, 2013). We carried out MD simulations with the phosphopeptide sequences derived from the V$_2$R, B$_2$R, and B$_2$R^{L370T}. All three peptides adopt an overall similar binding mode (Fig 6, middle panel), in which the phosphosensing pockets A, B, and C (Zhou *et al*, 2017) in

Figure 3.   Contribution of βarr1 in ERK1/2 phosphorylation for B$_2$R mutants.

(A–D) Knockdown of βarr1 leads to an increase in agonist-induced ERK1/2 phosphorylation for B$_2$R$^{\Delta G368}$ and B$_2$R$^{\Delta I374}$ but a decrease for B$_2$R^{L370T} and B$_2$R$^{\Delta G368/L370T}$ mutants. HEK-293 cells expressing the indicated B$_2$R mutants in the presence and absence of βarr1 knockdown were stimulated with indicated doses of bradykinin (Brady) for 10 min followed by detection of phosphorylated ERK1/2 using Western blotting. Densitometry-based quantification of data (mean ± SEM) from three independent experiments (five for B$_2$R$^{\Delta G368}$ and B$_2$R$^{\Delta I374}$) is presented as bar graphs in the lower panels. Data are normalized with respect to maximal dose under control condition (treated as 100%) and analyzed using two-way ANOVA with Bonferroni multiple comparisons test (*P < 0.05; **P < 0.01; ***P < 0.001).
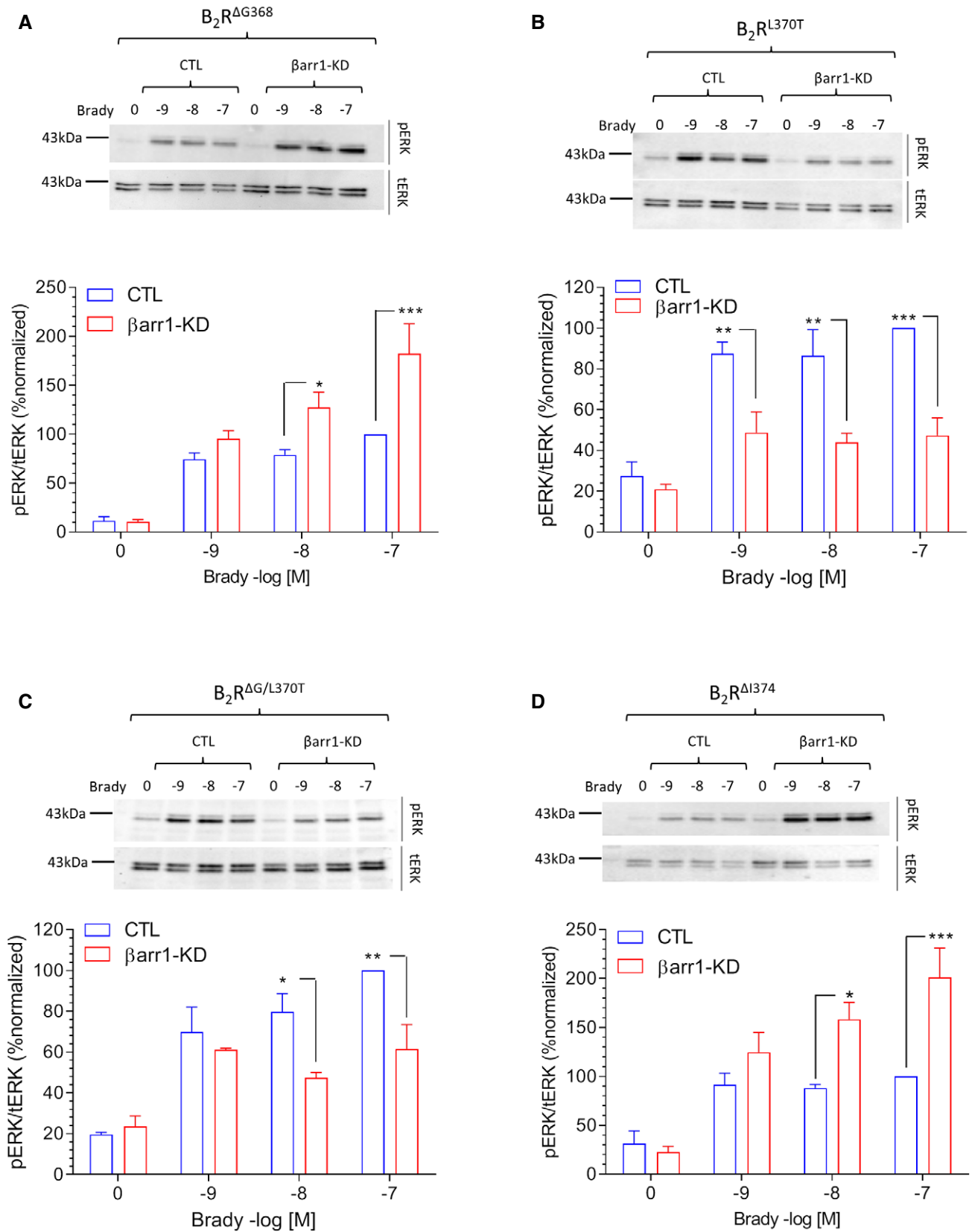
Figure 3.

βarr1 can accommodate the corresponding phospho-site patterns (Fig EV5A). The B$_2$R peptides display a loop bulging between S^{366} and M^{363} compared to the V$_2$R peptide, due to the presence of G^{368} (Fig EV5B). Furthermore, we observe that V$_2$R and B$_2$R^{L370T} peptides use two phosphorylated threonines, i.e., T^{359}/T^{360} and T^{369}/T^{370} to form a bifurcated electrostatic interaction with K^{294}
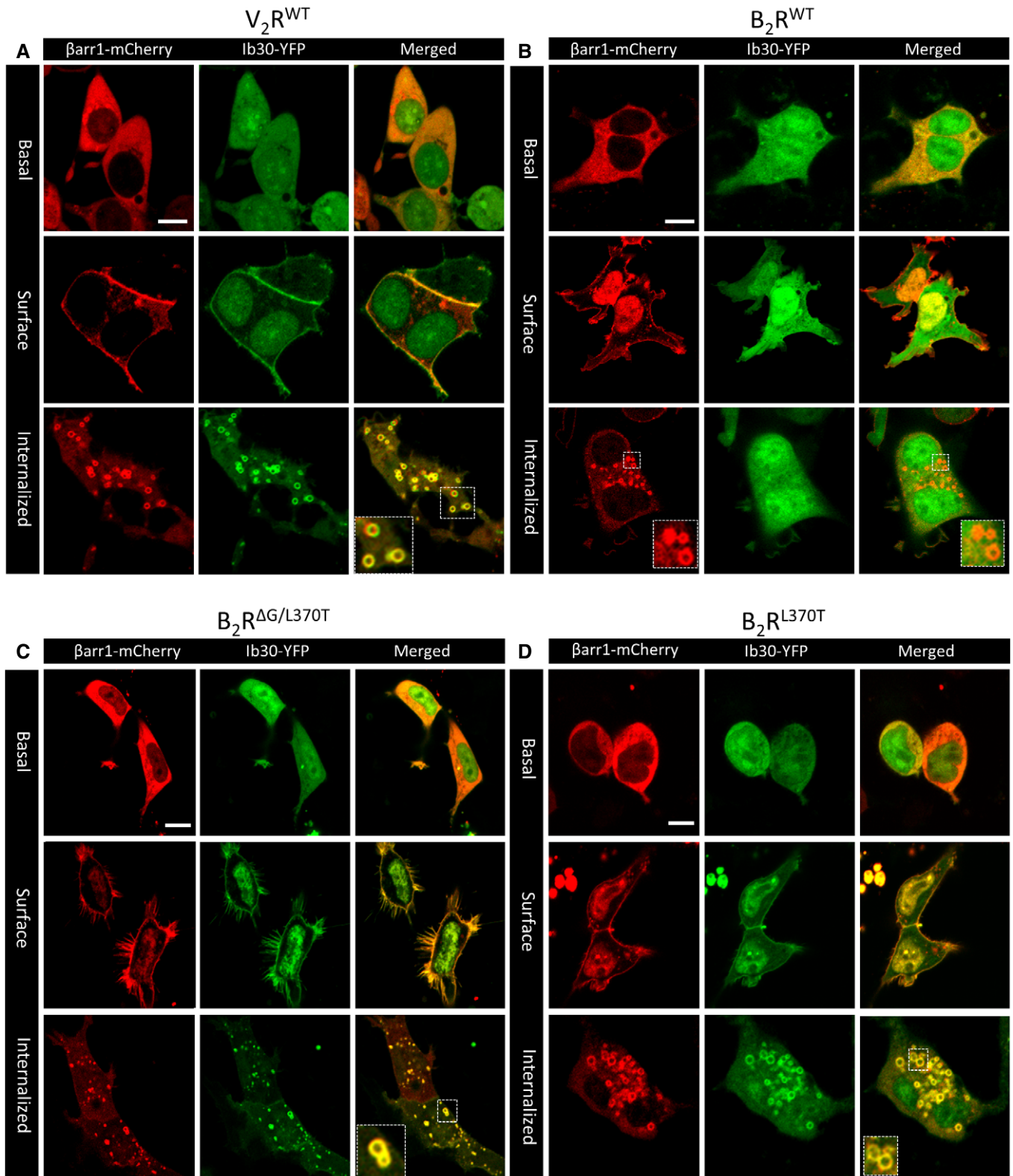

Figure 4.

Figure 4.   An intrabody sensor suggests distinct conformations of βarr1 for V₂R and B₂R.

(A–D) HEK-293 cells expressing V$_2$R, B$_2$R, B$_2$R$^{\Delta G368/L370T}$, or B$_2$R^{L370T} along with βarr1-mCherry and YFP-tagged intrabody30 (Ib30-YFP) were stimulated with their respective agonists (AVP, 100 nM for V$_2$R) and (bradykinin, 100 nM for B$_2$R) and the localization of βarr1 and Ib30 were visualized. Although βarr1 gets recruited for all four constructs, Ib30-YFP does not colocalize with βarr1 either at the surface or upon internalization in case of B$_2$R^{WT}. Representative data from 3–5 independent experiments are shown, and the scale bar is 10 μm. Visual scoring from 3–5 independent experiments revealed agonist-induced Ib30 recruitment (i.e., membrane and endosomal localization) in approximately 82% of the cells for V$_2$R (691 cells), 10% for B$_2$R^{WT} (254 cells), 63% for B$_2$R^{L370T} (273 cells), and 83% for B$_2$R$^{\Delta G368/L370T}$ (158 cells). Pearson's correlation coefficients (PCC) were measured to assess the colocalization of βarr1 and Ib30 using JACoP plugin in ImageJ, and the mean ± sem for the basal, surface, and internalized panels, respectively, are presented here. B$_2$R^{WT} — 0.32 ± 0.02 from 16 cells, 0.18 ± 0.01 from 32 cells, and 0.25 ± 0.02 from 31 cells; B$_2$R$^{\Delta G368/L370T}$ — 0.32 ± 0.03 from 13 cells, 0.92 ± 0.01 from 18 cells, and 0.90 ± 0.01 from 16 cells; B$_2$R^{L370T} — 0.26 ± 0.01 from 10 cells, 0.85 ± 0.01 from 11 cells, and 0.87 ± 0.01 from 25 cells.

in the lariat loop of βarr1 (Fig 6, upper panel). In contrast, the B$_2$R peptide is able to establish only a single interaction with K^{294} via the phosphorylated T^{369}, and the second interaction is not possible due to the presence of non-polar residue, i.e., L^{370} (Fig 6, upper panel). This is further corroborated by measuring the stability of these two salt bridges for different peptides in complex with βarr1 (Fig 6, lower panel).

We also observe that the presence or absence of a bifurcated connection between the peptides and K^{294} impact the conformational states of the lariat loop (Fig 6, lower panel). When present, the lariat loop preferentially samples conformations belonging to "Cluster 1" as seen for the V$_2$R and B$_2$R^{L370T} peptides; however, in its absence, the lariat loop conformations are shifted downwards favoring "Cluster2" as seen in the B$_2$R^{WT} peptide (Fig 6, lower panel). Overall, the "Cluster1" resembles the conformation of the lariat loop observed in the V$_2$Rpp-βarr1 crystal structure with an average rmsd of 1.9 Å; however, in "Cluster2", the average rmsd increases to 4.6 Å compared to the crystal structure (Fig 6, lower panel). These observations provide a structural framework to suggest that the relative orientation of the lariat loop in βarr1 is directed by the spatial pattern of phosphorylation sites present in GPCRs. While corroborating experimental evidence is still needed, it is tempting to speculate that the relative orientation of the lariat loop imparts conformational differences in βarr1, which are potentially linked to distinct functional outcomes. It would be interesting to measure a direct contribution of this salt bridge and the relative orientation of the lariat loop in the recruitment of βarr1, its conformational signature, and effect on ERK1/2 phosphorylation in future studies.

Engineering double-serine cluster reverses the contribution of βarr1 in ERK1/2 activation for AT$_{1a}$R

In order to further extend our findings, we next investigated the human angiotensin II type 1a receptor (AT$_{1a}$R). AT$_{1a}$R consists of two phospho-site patterns, which can be categorized as PXPXXP and PXXPXXP, similar to that present in the V$_2$R (Fig 7A).

Moreover, it also harbors a double-phospho-site cluster i.e. Ser^{335}/Thr^{336}, analogous to Thr^{359}/Thr^{360} in V$_2$R. Still however, similar to B$_2$R, siRNA-mediated βarr1 depletion leads to an augmentation of agonist-induced ERK1/2 phosphorylation (Ahn *et al*, 2004), which we also confirmed using shRNA mediated βarr1 knockdown (Fig 7C). Therefore, taking lead from the B$_2$R data, we focused on Leu^{337} in AT$_{1a}$R, and we generated two different mutants by either mutating Leu^{337} to Thr, i.e., AT$_{1a}$R^{L337T}, or by deleting Leu^{337}, i.e., AT$_{1a}$R$^{\Delta L337}$ (Fig 7B). These changes either disrupt the PXXPXXP pattern (i.e., in AT$_{1a}$R$^{\Delta L337}$) or leave it unchanged (i.e., in AT$_{1a}$R^{L337T}). Surface expressions of these mutants were comparable under the control vs. βarr1 knockdown conditions (Fig EV1D). In agonist-induced ERK1/2 phosphorylation assay, we observed that contrary to AT$_{1a}$R^{WT}, depletion of βarr1 resulted in a significant reduction of agonist-induced ERK1/2 phosphorylation for the AT$_{1a}$R^{L337T} and AT$_{1a}$R$^{\Delta L337}$ mutants (Fig 7D and E). This pattern is reminiscent of B$_2$R^{L370T} mutant, where a single point mutation (i.e., Leu^{370}Thr) reverses the contribution of βarr1 in ERK1/2 phosphorylation. Considering the distribution of multiple potential phosphorylation sites in AT$_{1a}$R, it should be possible to design additional mutants and probe their ERK1/2 phosphorylation pattern to deduce further insights into βarr1-mediated ERK1/2 activation. Nonetheless, taken together with B$_2$R data, our findings underscore the importance of spatially positioned key phosphorylation sites in the receptors in directing the role of βarr1 in ERK1/2 activation and also suggest that PXPXXP/PXXPXXP type patterns may not directly correlate with the contribution of βarr1 in ERK1/2 activation.

Discussion

The interaction of βarrs is mostly conserved across the GPCR family, but there are many instances of distinct functional contribution of βarrs in trafficking and signaling for different receptors (Shenoy & Lefkowitz, 2011; Kang *et al*, 2014; Srivastava *et al*, 2015). These functional differences are manifested even for those receptors, which display qualitatively similar βarr recruitment and trafficking

Figure 5.   βarr1 conformation and G-protein coupling for B₂R mutants.

A   HEK-293 cells expressing the indicated receptor constructs (pcDNA vector control for mock-transfection) together with SmBiT-βarr1 and LgBiT-Ib30 were stimulated with the indicated concentrations of respective agonists for 10 min. Subsequently, the luminescence signal generated upon the interaction of SmBiT-βarr1 and LgBiT-Ib30 was measured, normalized with basal signal (i.e., no-agonist stimulation treated as 1), and plotted using GraphPad Prism. pEC$_{50}$ (top) and E$_{max}$ (bottom) values are mentioned in the respective graphs, and data represent mean ± SEM of four independent experiments, each carried out in duplicate.

B   HEK-293 cells expressing the NanoBiT-Gq protein and indicated B$_2$R constructs were treated different concentrations of bradykinin, and ligand-induced change in luminescent signal was measured. Concentration-response curves were plotted using GraphPad Prism to calculate pEC$_{50}$ (top) and E$_{max}$ (bottom) values included in the graph. Data represent mean ± SEM of three independent experiments with each performed in duplicate and normalized with respect to the luminescence signal under basal (no-agonist treatment) condition (treated as 1).
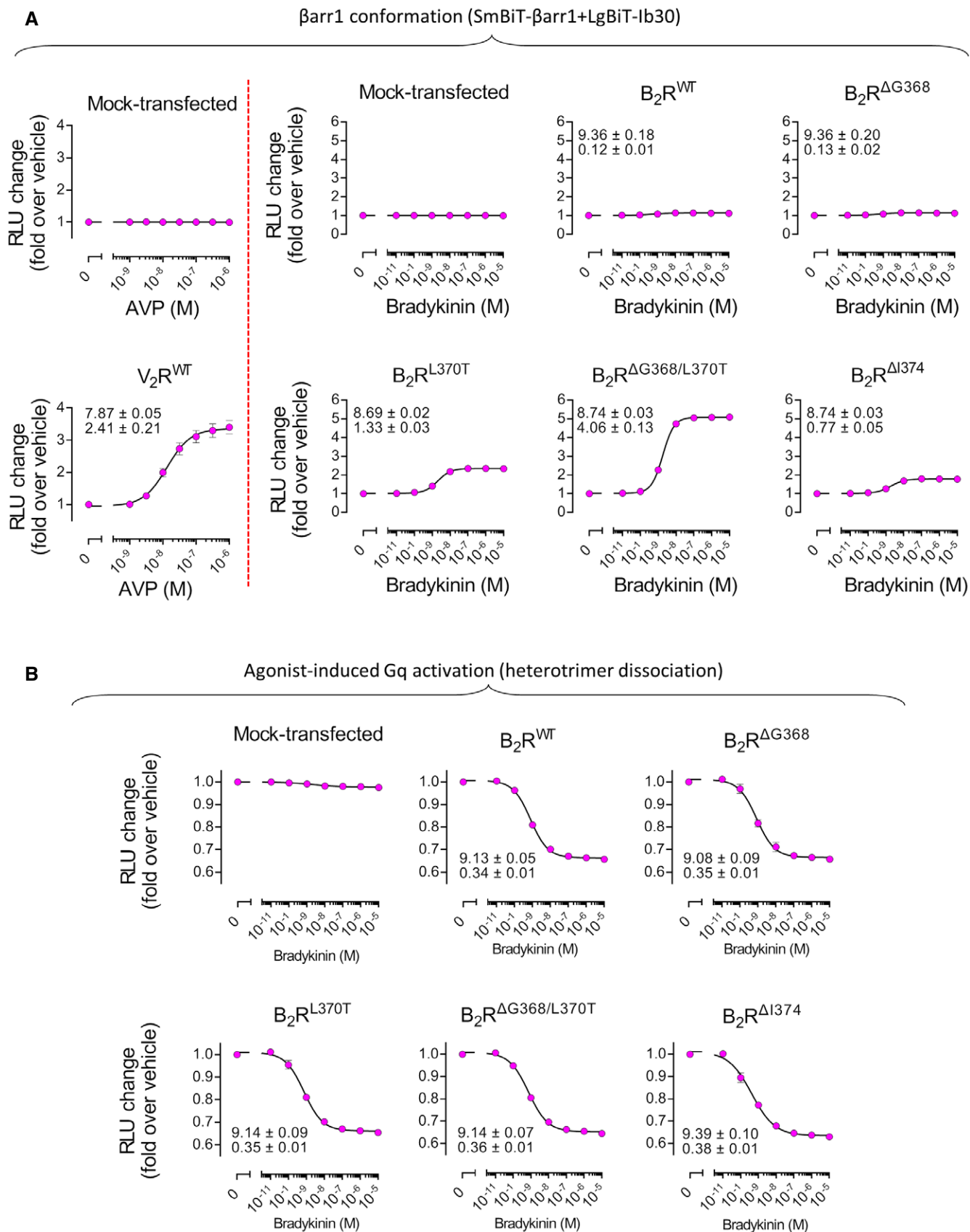
A

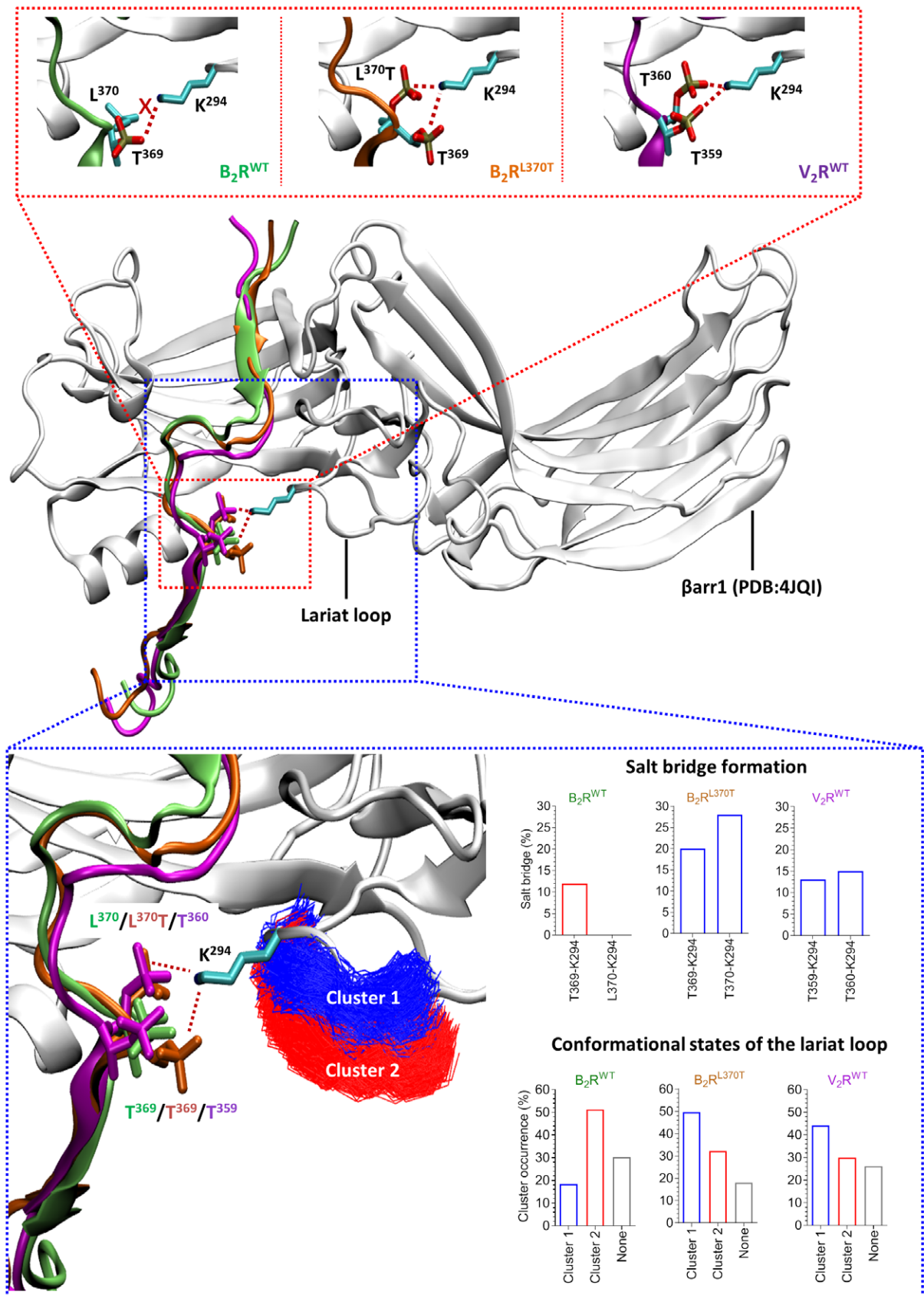βarr1 conformation (SmBiT-βarr1+LgBiT-Ib30)

B

Agonist-induced Gq activation (heterotrimer dissociation)

Figure 5.

Figure 6.

Figure 6. Structural insights into phospho-site interaction and βarr1 conformation.

Structural model of βarr1 in complex with phosphopeptides corresponding to the V_2R, B_2R, and B_2R^{L370T} were generated based on previously determined structure of V_2Rpp-βarr1 complex (middle panel). A bifurcated salt bridge links the V_2R and B_2R^{L370T} peptides to K^{294} in the lariat loop of βarr1 via T^{359}/T^{360} and T^{369}/T^{370}, respectively, but not in B_2R^{WT} peptide (upper panel). The frequency of salt bridge formation between the phospho-sites on the receptor and K^{294} in βarr1 was computed over 4 μs accumulated simulation time per complex using a distance threshold of 3.2 Å between the oxygen of the phosphate group of phosphorylated threonines and the protonated nitrogen of K^{294}. B_2R^{L370T} mutant establishes a bifurcated interaction with K^{294} in the lariat loop, analogous to that in V_2R peptide while B_2R peptide forms only a single salt bridge (lower panel). Differential lariat loop stabilization correlates with distinct conformational states. Simulations of 4 μs per complex were clustered with a rmsd cut-off of 2.2 Å yielding Cluster 1 and Cluster 2 while None reflects conformations that did not fulfill this condition. The phosphopeptides corresponding to V_2R and B_2R^{L370T} with a conserved bifurcated salt bridge adopt preferential conformational states belonging to Cluster 1 the B_2R^{WT} peptide with a single salt bridge favors the conformations of Cluster 2.

patterns (Ahn *et al*, 2004; Srivastava *et al*, 2015). Not only the differences in the phosphorylation patterns of different GPCRs can fine tune receptor-specific conformations and functional capabilities of βarrs (Lee *et al*, 2016; Nuber *et al*, 2016; Baidya *et al*, 2020) but also, differential phosphorylation patterns of a given GPCR can impart distinct conformational changes in recruited βarrs resulting in different functional responses (Charest *et al*, 2005; Shukla *et al*, 2008; Nobles *et al*, 2011; Zimmerman *et al*, 2012). These examples suggest that different GPCR-βarr complexes formed in cells, which may grossly look similar, do not necessarily encode identical functional outcomes. Our data presented here reveal that spatial positioning of key receptor phosphorylation sites can play a decisive role in the qualitative contribution of βarr1 in ERK1/2 activation. Our findings also underscore a conformational mechanism for this phenomenon via specific interactions between the key receptor phosphorylation sites and a conserved residue in βarr1.

An interesting point that also emerges from the current study is that βarr1 conformations supporting receptor trafficking vs. ERK1/2 phosphorylation may be different from each other. This is based on the observation that all three receptors tested here induce a similar pattern of agonist-induced βarr1 trafficking but the contribution of βarr1 in ERK1/2 activation is strikingly different. Going forward, it would be interesting to gather high-resolution structural information on these different receptor-βarr1 complexes to further illuminate structural and functional diversity in this signaling system. Recently, cryo-EM structures of three different GPCRs have been determined in complex with βarr1. These receptors include the human neurotensin receptor (NTS1R; Yin *et al*, 2019; Huang *et al*, 2020), the human muscarinic receptor (M2R; Staus *et al*, 2020) and the turkey β1-adrenergic receptor (β1AR; Lee *et al*, 2020). While comparing these structures with previously determined rhodopsin-visual-arrestin crystal structure (Zhou *et al*, 2017), an interesting observation emerges in terms of βarr1 orientation with respect to the membrane bilayer (Chaturvedi *et al*, 2020). βarr1 in the NTSR1-βarr1 complexes is rotated by about 85–90° in the plane of the membrane when compared to the rhodopsin-visual-arrestin structure, which is not observed in the M_2R-βarr1 and $β_1AR$-βarr1

structures (Chaturvedi *et al*, 2020). It would be very interesting to probe in future whether distinct phosphorylation patterns may direct specific βarr orientation in GPCR-βarr complexes, and if they have a direct impact on functional outcomes.

One of the key features driving the functional multiplicity of βarrs, including ERK1/2 activation, is their ability to interact with multiple binding partners and nucleate signalosomes (Lefkowitz & Shenoy, 2005; DeWire *et al*, 2007; Chen *et al*, 2018). For example, βarrs can scaffold c-Raf1, MEK1, and ERK2 to promote agonist-induced ERK1/2 phosphorylation (Lefkowitz & Shenoy, 2005; DeWire *et al*, 2007). Considering that engineering a double-Thr cluster in B_2R reverses the contribution of βarr1 in agonist-induced ERK1/2 phosphorylation, it would be tantalizing to probe in future studies how the scaffolding properties of βarr1 changes in the context of this modified pattern of receptor phosphorylation sites. Based on the differences observed in the reactivity pattern of intrabody sensor, it is tempting to speculate that distinct βarr1 conformations may encode differential scaffolding abilities for different binding partners and thereby, orchestrating the corresponding functional outcomes. However, this hypothesis remains to be experimentally explored in subsequent studies. We have focused our study on βarr1, which displays opposite contribution in ERK1/2 activation for V_2R vs. B_2R and $AT_{1a}R$. βarr2 on the other hand has qualitatively similar contribution for all three receptors, i.e., its knockdown results to a decrease in ERK1/2 activation. This reciprocal regulation of βarr isoforms has been investigated and discussed earlier [14]. In this previous study, authors have systematically evaluated the underlying mechanism for potentiation of ERK1/2 response upon βarr1 knockdown and conclude that it is primarily due to an augmentation of βarr2-dependent activation of ERK1/2. They also conclude that endogenous βarr1 present at relatively higher levels than βarr2 in HEK-293 cells essentially exerts a dominant-negative effect on βarr2 mediated ERK1/2 phosphorylation. Although both βarr1 and 2 are recruited to the receptor, βarr2 is potentially a better scaffold for the components of ERK1/2 cascade and, therefore, βarr1 depletion results in enhanced ERK1/2 phosphorylation.

Figure 7. Contribution of βarr1 in ERK1/2 phosphorylation for $AT_{1a}R$ mutants.

A   Phospho-site clusters in the carboxyl-terminus of V_2R and $AT_{1a}R$ are underlined and color-coded to reflect the PXPXXP and PXXPXXP patterns as proposed in a previous study (Zhou *et al*, 2017).

B   Two different $AT_{1a}R$ mutants were generated by site-directed mutagenesis to mimic the spatial distribution of Ser/Thr as in V_2R with respect to double-Thr cluster. The red dotted box highlights the resulting sequence upon either the deletion of Leu^{337} or $Leu^{337}Thr$ mutation.

C–E HEK-293 cells expressing the indicated $AT_{1a}R$ constructs, in the absence (CTL; control) or presence of βarr1 knockdown (βarr1-KD) were stimulated with indicated concentrations of angiotensin II (AngII) for 10 min. Subsequently, ERK1/2 phosphorylation was measured by Western blotting and signal intensities were quantified using densitometry and presented as bar graphs. Data were normalized with respect to the signal at 100 nM agonist concentration in control cells (treated as 100%) and represent mean ± SEM of five (six for $AT_{1a}R^{ΔL337}$) independent experiments. Data were analyzed using two-way ANOVA with Bonferroni multiple comparisons test (***$P < 0.001$, *$P < 0.05$).
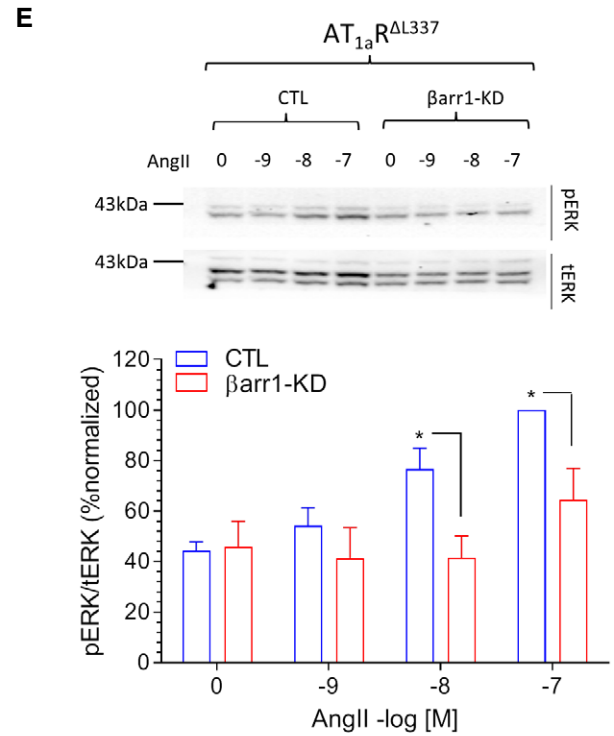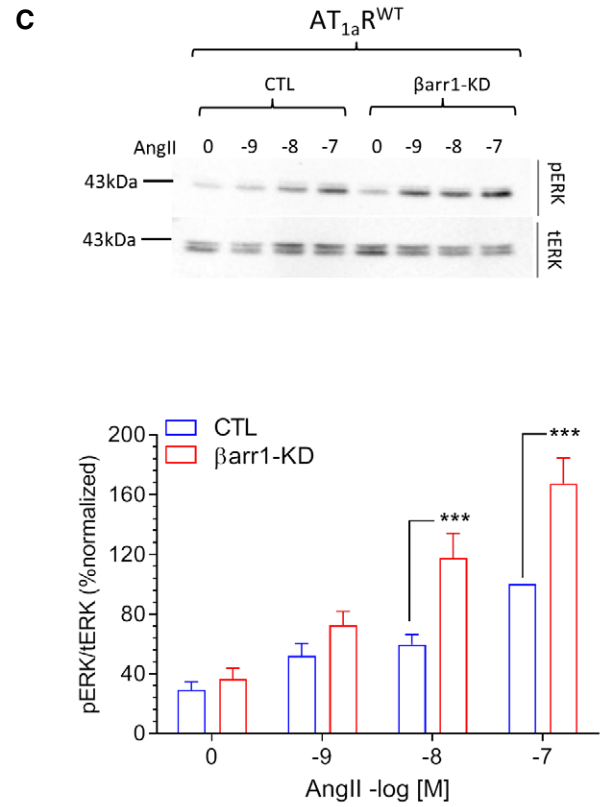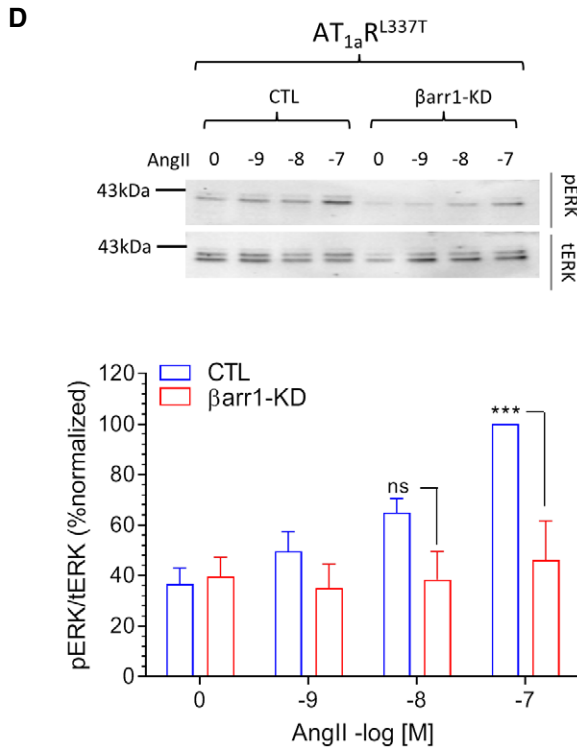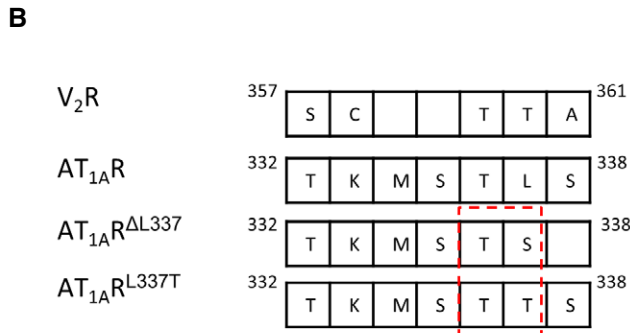
A

V$_2$R ^{341}CCARGRTPPSLGPQDESCTTASSSLAKDTSS^{371}

SCTTAS [PXPXXP]

SCTTASS [PXXPXXP]

AT$_{1a}$R ^{321}PPKAKSHSNLSTKMSTLSYRPSDNVSSSTKK^{351}

SHSNLS [PXPXXP]

TKMSTLS [PXXPXXP]

B

V$_2$R 357	S	C		T	T	A 361
AT$_{1A}$R 332	T	K	M	S	T	L	S 338
AT$_{1A}$R^{ΔL337} 332	T	K	M	S	T	S	338
AT$_{1A}$R^{L337T} 332	T	K	M	S	T	T	S 338

C

D

E

Figure 7.

Although engineering specific phosphorylation sites in the receptors studied here has functional effects, the phosphorylation status of these sites in cellular and physiological context remains to be experimentally established. Moreover, as different sites in GPCRs can be phosphorylated by different GRKs and other kinases, it would be interesting to explore such a possibility for the receptors used here, and probe if that has a role in differential contribution of βarr1 in ERK1/2 activation. It is also worth noting that although the orientation of lariat loop and the propensity of salt bridge formation with Lys^{294} appear to differ between V_2R and B_2R, future studies are required to correlate it directly with the inhibitory or promotive nature of βarr1 in ERK1/2 phosphorylation. The crystal structure of V_2Rpp-βarr1 complex suggests that the interaction of the phosphate groups in the double-Thr cluster (T^{359}/T^{360}) of V_2Rpp with Lys^{294} is involved in the disruption of the polar core in βarr1, which is an important step in βarr activation. Thus, it is tempting to speculate that different degrees of polar core disruption in βarr1, for example, between V_2R and B_2R, may link the ensuing βarr1 conformation with corresponding ERK1/2 activation. Finally, it is worth mentioning that some recent studies have proposed that the contribution of βarrs in ERK1/2 phosphorylation may not be completely independent of G proteins, and instead an interplay of G proteins and βarrs may be involved (O'Hayre et al, 2017; Grundmann et al, 2018; Gurevich & Gurevich, 2018a; Gutkind & Kostenis, 2018; Luttrell et al, 2018). Although we are not probing this aspect in the current study, our finding provide an additional framework and offer phospho-site mutants of these receptors as additional tools to delineate the interplay of G proteins and βarrs in agonist-induced ERK1/2 activation.

In summary, we discover that spatial positioning of the key phosphorylation sites in selected GPCRs triggers the role reversal of βarr1 in agonist-induced ERK1/2 activation. Our study also identifies the critical involvement of a bifurcated salt bridge interaction between a double-phospho-site cluster on the receptor and a conserved lysine residue in βarr1, which directs the orientation of the lariat loop in βarr1. These findings provide a previously missing mechanistic link for the opposite contribution of βarr1 in ERK1/2 activation for different GPCRs, and thereby, improve the current framework of βarr-dependent GPCR signaling and biased agonism.

Materials and Methods

General reagents, plasmid constructs, and cell culture

HEK-293 cells (ATCC) were cultured and maintained in DMEM (Thermo Fisher) supplemented with 10% FBS and 100 U/ml penicillin and 100 μg/ml streptomycin. The cells were cultured in sterile 10-cm plates at 37°C under 5% CO_2 and passaged at 70–80% confluency. For transfection, 50–60% confluent cells were transfected with desired DNA using PolyEthylenImine (PEI) as transfection reagent at the DNA:PEI ratio of 1:3. Expression plasmids for V_2R, B_2R, $AT_{1a}R$, Ib30-YFP, βarr1 shRNA, and βarr1-mCherry have been described previously (Kumari et al, 2016, 2017; Ghosh et al, 2017, 2019; Pandey et al, 2019a; Baidya et al, 2020). Receptor mutants were generated using site-directed mutagenesis kit (NEB) and sequenced (Macrogen) before use in the experiments. Commercial antibodies used in various assays are described in the corresponding sections below.

Surface expression of receptor constructs

Surface expression of various GPCRs used in this study was measured using whole cell surface ELISA assay as described previously (Pandey et al, 2019b). In brief, after 24 h of transfection, cells were seeded onto poly-D-lysine–coated 24-well plates at a density of 100,000 cells/well and allowed to adhere for an additional 24 h. Subsequently, the cells were serum starved for 4–6 h and then fixed with 4% formaldehyde for 20 min. Cells were washed three times with 1× TBS, non-specific sites were blocked for 1 h with 1%BSA in 1× TBS and incubated with HRP-coupled anti-FLAG M2 antibody (Sigma, cat. no. A8592, 1:5,000 dilution). After three washes, TMB substrate was added to each well, and once the color was developed, the reaction was stopped by adding 100 μl 1 M H_2SO_4. The absorbance was measured at 450 nm using a multi-plate reader (Victor X4, Perkin Elmer). Cell density per well was determined by staining with 0.2% Janus Green and measuring absorbance at 595 nm. Normalized surface expression was calculated by the ratio of A_{450}/A_{595}.

Confocal microscopy

In order to visualize agonist-induced trafficking of βarr1-mCherry, and the reactivity of Ib30-YFP with βarr1 for different receptor constructs, we used confocal microscopy as described earlier (Baidya et al, 2020). Briefly, HEK-293 cells were co-transfected with either, the receptor and βarr1-mCherry, or receptor, βarr1-mCherry and Ib30-YFP, and 24 h post-transfection, they were seeded onto poly-D-lysine–coated confocal dishes. After another 24 h, cells were serum starved for 4–6 h and then stimulated with respective agonists at indicated concentrations. Live cell imaging was performed using Zeiss LSM 710 NLO confocal microscope attached to a 32× array GaAsP descanned detector (Zeiss). A Multiline Argon laser for YFP (488 nm) and a Diode Pump Solid State Laser for mCherry (561 nm) were used. Intensity of laser and pinhole settings were maintained in the same range for any parallel set of experiments and filter excitation regions and bandwidths were adjusted to avoid any spectral overlap between the two channels. Images were finally processed in ZEN lite (ZEN-blue/ZEN-black) software suite from ZEISS. Agonist-induced trafficking of βarr1-mCherry was quantified across multiple cells from independent experiments by manually counting surface (membrane) and endosomal (internalized) localization patterns. Colocalization of βarr1-mCherry and Ib30-YFP were measured using either manually, by a line-scan analysis in ImageJ to measure fluorescence intensities across a drawn line, or by using the JACoP (Just Another Colocalization Plugin) tool in ImageJ (Bolte & Cordelieres, 2006) to calculate Pearson's correlation coefficient (PCC).

NanoBiT-G-protein dissociation assay

Ligand-induced Gq dissociation was measured by a NanoBiT-G-protein dissociation assay (Inoue et al, 2019), in which interaction between a Gα subunit and a Gβγ subunit was monitored by a NanoLuc-based enzyme complementation system called NanoBiT (Promega). Specifically, a NanoBiT-Gq protein consisting of Gαq subunit fused with a large fragment (LgBiT) in the alpha helical domain and an N-terminally small fragment (SmBiT)-fused Gβ1 was expressed along with untagged Gγ2 subunit with a C68S mutation,

RIC8A, and a test B_2R construct. HEK-293A cells (Thermo Fisher Scientific) were seeded in a 6-well culture plate at a concentration of 2×10^5 cells/ml (2 ml per well in DMEM (Nissui) supplemented with 10% fetal bovine serum (Gibco), glutamine, penicillin, and streptomycin) 1-day before transfection. Transfection solution was prepared by combining 5 μl (per well in a 6-well plate hereafter) of polyethylenimine Max solution (Polysciences; 1 mg/ml), 200 μl of Opti-MEM (Thermo Fisher Scientific) and a plasmid mixture consisting of 200 ng B_2R construct, 100 ng LgBiT-containing Gαq subunit, 500 ng SmBiT-Gβ1, 500 ng Gγ2 (C68S), and 100 ng RIC8A. After incubation for 1 day, the transfected cells were harvested with 0.5 mM EDTA-containing Dulbecco's PBS, centrifuged, and suspended in 2 ml of HBSS containing 0.01% bovine serum albumin (BSA; fatty acid–free grade; SERVA) and 5 mM HEPES (pH 7.4) (assay buffer). The cell suspension was dispensed in a white 96-well plate at a volume of 80 μl per well and loaded with 20 μl of 50 μM coelenterazine (Carbosynth) diluted in the assay buffer. After 2-h incubation at room temperature, the plate was measured for baseline luminescence (Spectramax L, Molecular Devices) and a titrated Bradykinin (20 μl; 6× of final concentrations) were manually added. The plate was immediately read at room temperature for the following 10 min as a kinetics mode at a measurement interval of 20 s. The luminescence counts over 5–10 min after ligand addition were averaged and normalized to the initial count. The fold-change values were further normalized to that of vehicle-treated samples and were used to plot G-protein dissociation response. Using Prism 8 software (GraphPad Prism), the G-protein dissociation signals were fitted to a four-parameter sigmoidal concentration–response curve, from which pEC_{50} values (negative logarithmic values of EC_{50} values) and E_{max} values were used to calculate mean and SEM.

NanoBiT-β-arrestin recruitment assay

Ligand-induced β-arrestin recruitment to GPCR was measured by a NanoBiT-β-arrestin recruitment assay (Dixon *et al*, 2016; Shihoya *et al*, 2018), which assesses enzyme complementation of a C-terminally SmBiT-fused B_2R construct (B_2R-Sm) with N-terminally LgBiT-fused β-arrestin (Lg-βarr). FLAG-B_2R was C-terminally fused to SmBiT with a 15-amino acid flexible linker (GGSGGG GSGGSSSGG) and inserted into a pCAGGS mammalian expression plasmid. Transfection in HEK293A cells was performed as described in the NanoBiT-G-protein dissociation assay by using a plasmid mixture consisting of a test B_2R-Sm construct (500 ng) and Lg-βarr1 (100 ng). Next day, the transfected cells were subjected to the same assay procedure as described above and increase in luminescent signal was measured.

NanoBiT-Ib30 assay

Ligand-induced β-arrestin conformational change was measured by a NanoBiT-Ib30 assay, which was developed in this work. Ib30 was N-terminally fused to LgBiT (codon-optimized and gene-synthesized by Genscript) with the 15-amino acid flexible linker and inserted into the pCAGGS plasmid. Similarly, human β-arrestin1 was N-terminally fused to SmBiT with the 15-amino acid flexible linker and inserted into the pCAGGS plasmid. Transfection in HEK293A cells was performed as described in the NanoBiT-G-protein dissociation assay by using a plasmid mixture

consisting of a test B_2R construct (200 ng), Sm-βarr1 (100 ng), and Lg-Ib30 (500 ng). For a control experiment, a V_2R-encoding plasmid (200 ng) or an empty plasmid was used in place of a B_2R plasmid. Next day, the transfected cells were subjected to the same assay procedure as described above and increase in luminescent signal was measured.

ERK1/2 phosphorylation assay

For measuring agonist-induced ERK1/2 phosphorylation, we used HEK-293 cells with βarr1 knockdown using either shRNA (Ghosh *et al*, 2019) or CRISPR/Cas9 approach (Luttrell *et al*, 2018) and followed the protocol described previously (Beautrait *et al*, 2017). For shRNA approach (Figs 1C and D, 3 and 7B–E), about three million HEK-293 cells stably expressing either an shRNA against βarr1 or a control shRNA were transfected at approximately 60% confluency with the indicated receptor constructs. We used 0.5, 1, and 2 μg of V_2R, B_2R, and $AT_{1a}R$ constructs, respectively, and after 24 h, one million cells were seeded into each well of 6-well plates. Forty-eight hours post-transfection, cells were serum starved for 4–6 h in DMEM supplemented with 20 mM HEPES and 0.01% BSA, stimulated with indicated concentrations of the corresponding agonists, and subsequently, lysed using 2× SDS loading buffer followed by boiling at 95°C for 15 min. Phosphorylated and total levels of ERK1/2 were measured by Western blotting using anti-pERK1/2 and anti-total ERK1/2 primary antibodies (CST, cat. no. 9101; and 9102, respectively; 1:5,000 dilution) and HRP-coupled anti-rabbit secondary antibody (GenScript, cat. no. A00098). Blots were developed using HRP substrate from Promega and Chemi-Documentation system from Bio-Rad. Densitometry-based quantification of bands was carried out using Bio-Rad software or ImageJ and plotted in GraphPad Prism.

For CRISPR/Cas9-based βarr1/2-deleted HEK293 cells (Luttrell *et al*, 2018) (Fig EV2), about 1.5 million cells were seeded on a 10-cm cell culture plate a day prior to transfection to achieve ~80% confluency. 1 μg of B_2R, $B_2R^{ΔG368/L370T}$ or B_2R^{L370T} constructs were transfected along with 0.3 μg of FLAG-βarr2, with or without 0.3 μg of FLAG-βarr1 (Beautrait *et al*, 2017). After 24 h, one million cells per well were seeded on to a 6-well plate. Forty-eight hours post-transfection, cells were serum starved, stimulated with or without 100 nM bradykinin (BK) for 10 min, followed by sample preparation and Western blotting as mentioned above. Here, HRP-coupled anti-rabbit secondary antibody from Bio-Rad was used (cat. no. 1706515). The expression of transfected βarr1 was detected using A1CT primary antibody (1:2,000 dilution; gifted by the Lefkowitz lab).

Molecular dynamics simulation

In order to generate the complexes of B_2Rpp^{WT}, B_2Rpp^{L370T}, and V_2Rpp^{WT}, we used the previously determined structure of V_2Rpp in complex with βarr1 (PDB code: 4JQI). Missing fragments in the βarr1 and V_2Rpp structures were modeled using the loop modeler module available in the MOE package (https://www.chemcomp. com). In addition, the co-crystallized Fab30 was also removed from the structural template. For modeling the binding of the B_2R^{WT} and B_2R^{370T} peptide sequences to βarr1, we considered two different alignments as indicated below:

Here, the residues numbers are indicated based on the corresponding receptor sequences, and the site for B_2R mutation (i.e., $L^{370}T$) is colored in red. Both models were obtained by converting the sequence of the V_2Rpp into that of the B_2Rpp and the corresponding B_2Rpp mutant. In alignment A, the studied mutation site 370 is located in the space corresponding to residue 360 in the V_2R/βarr1 complex. In this alignment, the G^{368} represents an insertion in the loop formed between the first and second β-sheet. The additional residue results in a loop extension in B_2Rpp and B_2Rpp^{L370T} compared to V_2Rpp, which can be appreciated in Fig EV5. In such a configuration, the $L^{370}T$ mutation in the B_2R interacts with residue K^{294} in the lariat loop and mediates key interactions between the N- and C-domain of βarr1. This structurally pivotal role could help explain the dramatic functional shift associated with a $L^{370}T$ mutation, i.e., supportive role of βarr1 in ERK1/2 phosphorylation. In alignment B, $L^{370}T$ is positioned such that it cannot interact with K^{294} but instead, interacts with K^{10}. Gaining this additional interaction in comparison with the B_2R^{WT} is likely result in an increased stabilization of the peptide. However, it is less likely to yield a significant change in the structure of peptide-βarr1 complex, as it is not located in the critical interface area of the N- and C-domain of βarr1. Based on this reasoning, our experimental observation in terms of ERK1/2 phosphorylation for different B_2R mutants, we proceeded with alignment A in our simulation studies.

The complexes were solvated in TIP3P water, with the ionic strength kept at 0.15 M using NaCl ions. Simulation parameters were obtained from the Charmm36M forcefield (Huang *et al*, 2017). Systems generated this way were simulated using the ACEMD software package (Harvey *et al*, 2009). To allow rearrangement of waters and side chains, we carried out a 25 ns equilibration phase in NPT conditions with restraints applied to backbone atoms. The time step was set to 2 fs and the pressure was kept constant, using the Berendsen barostat. After the equilibration, systems were simulated in NVT conditions for 1 μs in four parallel runs employing a 4 fs time step. For all runs, temperature was kept at 300 K using the Langevin thermostat and hydrogen bonds were restrained using the RATTLE algorithm. Non-bonded interactions were cut off at 9 Å with a smooth switching function applied at 7.5 Å. Before carrying out the structural analysis, simulation frames were aligned using the backbone atoms of the βarr1. To assess the magnitude of salt bridge formation between phosphorylated threonines (pT) residues and K^{294}, we quantified frames in which the protonated nitrogen of K^{294} and oxygens of the phosphate group of each respective pT were in a distance of <3.2 Å. Conformational variability of the lariat loop was studied with the clustering tool available in VMD (Humphrey *et al*, 1996). As a clustering parameter, we used RMSD (cut-off: 2.2) of the backbone atoms of residues 293 to 297 within the lariat loop.

Statistical analysis and data presentation

Quantified data were plotted and analyzed using GraphPad Prism software, and the details of experimental replicates and statistical analysis

are mentioned in the corresponding figure legends. Independent experiments mentioned in the figure legends indicate biological replicates.

Data availability

Data included in this manuscript are available from the authors upon reasonable request. No primary datasets have been generated or deposited.

Expanded View for this article is available online.

Conflict of interest

The authors declare that they have no conflict of interest.

Author contributions

Experiment design: AKS, AI, JS, SAL; Experiment and data analysis: AKS, AI, JS, SAL, MB, PK, HD-A, SP, MC, TMS, KK, YC; Manuscript writing: AKS; Funding: AKS, AI, JS, SAL; Study coordination and supervision: AKS.

References

Ahn S, Wei H, Garrison TR, Lefkowitz RJ (2004) Reciprocal regulation of angiotensin receptor-activated extracellular signal-regulated kinases by beta-arrestins 1 and 2. *J Biol Chem* 279: 7807 – 7811

Appleton KM, Luttrell LM (2013) Emergent biological properties of arrestin pathway-selective biased agonism. *J Recept Signal Transduct Res* 33: 153 – 161

Azzi M, Charest PG, Angers S, Rousseau G, Kohout T, Bouvier M, Pineyro G (2003) Beta-arrestin-mediated activation of MAPK by inverse agonists reveals distinct active conformations for G protein-coupled receptors. *Proc Natl Acad Sci USA* 100: 11406–11411

Baidya M, Kumari P, Dwivedi-Agnihotri H, Pandey S, Sokrat B, Sposini S, Chaturvedi M, Srivastava A, Roy D, Hanyaloglu AC, *et al* (2020) Genetically encoded intrabody sensors report the interaction and trafficking of beta-arrestin 1 upon activation of G protein-coupled receptors. *J Biol Chem* https://doi.org/10.1074/jbc.RA120.013470

Beautrait A, Paradis JS, Zimmerman B, Giubilaro J, Nikolajev L, Armando S, Kobayashi H, Yamani L, Namkung Y, Heydenreich FM, *et al* (2017) A new inhibitor of the beta-arrestin/AP2 endocytic complex reveals interplay between GPCR internalization and signalling. *Nat Commun* 8: 15054

Bockaert J, Pin JP (1999) Molecular tinkering of G protein-coupled receptors: an evolutionary success. *EMBO J* 18: 1723–1729

Bolte S, Cordelieres FP (2006) A guided tour into subcellular colocalization analysis in light microscopy. *J Microsc-Oxford* 224: 213–232

Charest PG, Terrillon S, Bouvier M (2005) Monitoring agonist-promoted conformational changes of beta-arrestin in living cells by intramolecular BRET. *EMBO Rep* 6: 334–340

Charest PG, Oligny-Longpre G, Bonin H, Azzi M, Bouvier M (2007) The V2 vasopressin receptor stimulates ERK1/2 activity independently of heterotrimeric G protein signalling. *Cell Signal* 19: 32–41

Chaturvedi M, Maharana J, Shukla AK (2020) Terminating G-protein coupling: structural snapshots of GPCR-beta-arrestin complexes. *Cell* 180: 1041–1043

Chen Q, Iverson TM, Gurevich VV (2018) Structural basis of Arrestin-dependent signal transduction. *Trends Biochem Sci* 43: 412–423

DeWire SM, Ahn S, Lefkowitz RJ, Shenoy SK (2007) Beta-arrestins and cell signaling. *Annu Rev Physiol* 69: 483–510

Dixon AS, Schwinn MK, Hall MP, Zimmerman K, Otto P, Lubben TH, Butler BL, Binkowski BF, Machleidt T, Kirkland TA, *et al* (2016) Nanoluc complementation reporter optimized for accurate measurement of protein interactions in cells. *ACS Chem Biol* 11: 400–408

Freedman NJ, Lefkowitz RJ (1996) Desensitization of G protein-coupled receptors. *Recent Prog Horm Res* 51: 319–351

Gesty-Palmer D, Yuan L, Martin B, Wood WH 3rd, Lee MH, Janech MG, Tsoi LC, Zheng WJ, Luttrell LM, Maudsley S (2013) beta-arrestin-selective G protein-coupled receptor agonists engender unique biological efficacy in vivo. *Mol Endocrinol* 27: 296–314

Ghosh E, Srivastava A, Baidya M, Kumari P, Dwivedi H, Nidhi K, Ranjan R, Dogra S, Koide A, Yadav PN, *et al* (2017) A synthetic intrabody-based selective and generic inhibitor of GPCR endocytosis. *Nat Nanotechnol* 12: 1190–1198

Ghosh E, Dwivedi H, Baidya M, Srivastava A, Kumari P, Stepniewski T, Kim HR, Lee MH, van Gastel J, Chaturvedi M, *et al* (2019) Conformational sensors and domain swapping reveal structural and functional differences between beta-Arrestin isoforms. *Cell Rep* 28: 3287–3299

Grundmann M, Merten N, Malfacini D, Inoue A, Preis P, Simon K, Ruttiger N, Ziegler N, Benkel T, Schmitt NK, *et al* (2018) Lack of beta-arrestin signaling in the absence of active G proteins. *Nat Commun* 9: 341

Gurevich VV, Gurevich EV (2004) The molecular acrobatics of arrestin activation. *Trends Pharmacol Sci* 25: 105–111

Gurevich VV, Gurevich EV (2018a) Arrestin-mediated signaling: is there a controversy? *World J Biol Chem* 9: 25–35

Gurevich VV, Gurevich EV (2018b) GPCRs and signal transducers: interaction stoichiometry. *Trends Pharmacol Sci* 39: 672–684

Gutkind JS, Kostenis E (2018) Arrestins as rheostats of GPCR signalling. *Nat Rev Mol Cell Biol* 19: 615–616

Harvey MJ, Giupponi G, Fabritiis GD (2009) ACEMD: accelerating biomolecular dynamics in the microsecond time scale. *J Chem Theory Comput* 5: 1632–1639

Huang J, Rauscher S, Nawrocki G, Ran T, Feig M, de Groot BL, Grubmuller H, MacKerell AD Jr (2017) CHARMM36m: an improved force field for folded and intrinsically disordered proteins. *Nat Methods* 14: 71–73

Huang W, Masureel M, Qu Q, Janetzko J, Inoue A, Kato HE, Robertson MJ, Nguyen KC, Glenn JS, Skiniotis G, *et al* (2020) Structure of the neurotensin receptor 1 in complex with beta-arrestin 1. *Nature* 579: 303–308

Humphrey W, Dalke A, Schulten K (1996) VMD: visual molecular dynamics. *J Mol Graph* 14: 33–38, 27–38

Inoue A, Raimondi F, Kadji FMN, Singh G, Kishi T, Uwamizu A, Ono Y, Shinjo Y, Ishida S, Arang N, *et al* (2019) Illuminating G-protein-coupling selectivity of GPCRs. *Cell* 177: 1933–1947

Kang DS, Tian X, Benovic JL (2014) Role of beta-arrestins and arrestin domain-containing proteins in G protein-coupled receptor trafficking. *Curr Opin Cell Biol* 27: 63–71

Kim J, Ahn S, Ren XR, Whalen EJ, Reiter E, Wei H, Lefkowitz RJ (2005) Functional antagonism of different G protein-coupled receptor kinases for beta-arrestin-mediated angiotensin II receptor signaling. *Proc Natl Acad Sci USA* 102: 1442–1447

Kumari P, Srivastava A, Banerjee R, Ghosh E, Gupta P, Ranjan R, Chen X, Gupta B, Gupta C, Jaiman D, *et al* (2016) Functional competence of a partially engaged GPCR-beta-arrestin complex. *Nat Commun* 7: 13416

Kumari P, Srivastava A, Ghosh E, Ranjan R, Dogra S, Yadav PN, Shukla AK (2017) Core engagement with beta-arrestin is dispensable for agonist-induced vasopressin receptor endocytosis and ERK activation. *Mol Biol Cell* 28: 1003–1010

Lee MH, Appleton KM, Strungs EG, Kwon JY, Morinelli TA, Peterson YK, Laporte SA, Luttrell LM (2016) The conformational signature of beta-arrestin2 predicts its trafficking and signalling functions. *Nature* 531: 665–668

Lee YWT, Nehmé R, Pandey S, Dwivedi-Agnihotri H, Chaturvedi M, Edwards PC, García-Nafría J, Leslie AGW, Shukla AK, Tate CG (2020) Molecular determinants of β-arrestin coupling to formoterol-bound β1-adrenoceptor. *Nature* https://doi.org/10.1038/s41586-020-2419-1

Lefkowitz RJ, Shenoy SK (2005) Transduction of receptor signals by beta-arrestins. *Science* 308: 512–517

Luttrell LM, Gesty-Palmer D (2010) Beyond desensitization: physiological relevance of arrestin-dependent signaling. *Pharmacol Rev* 62: 305–330

Luttrell LM, Wang J, Plouffe B, Smith JS, Yamani L, Kaur S, Jean-Charles PY, Gauthier C, Lee MH, Pani B, *et al* (2018) Manifold roles of beta-arrestins in GPCR signaling elucidated with siRNA and CRISPR/Cas9. *Sci Signal* 11: eaat7650

Nobles KN, Xiao K, Ahn S, Shukla AK, Lam CM, Rajagopal S, Strachan RT, Huang TY, Bressler EA, Hara MR, *et al* (2011) Distinct phosphorylation sites on the beta(2)-adrenergic receptor establish a barcode that encodes differential functions of beta-arrestin. *Sci Signal* 4: ra51

Nuber S, Zabel U, Lorenz K, Nuber A, Milligan G, Tobin AB, Lohse MJ, Hoffmann C (2016) beta-Arrestin biosensors reveal a rapid, receptor-dependent activation/deactivation cycle. *Nature* 531: 661–664

Oakley RH, Laporte SA, Holt JA, Caron MG, Barak LS (2000) Differential affinities of visual arrestin, beta arrestin1, and beta arrestin2 for G protein-coupled receptors delineate two major classes of receptors. *J Biol Chem* 275: 17201–17210

O'Hayre M, Eichel K, Avino S, Zhao X, Steffen DJ, Feng X, Kawakami K, Aoki J, Messer K, Sunahara R, *et al* (2017) Genetic evidence that beta-arrestins

are dispensable for the initiation of beta2-adrenergic receptor signaling to ERK. *Sci Signal* 10: eaal3395

Oligny-Longpre G, Corbani M, Zhou J, Hogue M, Guillon G, Bouvier M (2012) Engagement of beta-arrestin by transactivated insulin-like growth factor receptor is needed for V2 vasopressin receptor-stimulated ERK1/2 activation. *Proc Natl Acad Sci USA* 109: E1028 – E1037

Pandey S, Li XX, Srivastava A, Baidya M, Kumari P, Dwivedi H, Chaturvedi M, Ghosh E, Woodruff TM, Shukla AK (2019a) Partial ligand-receptor engagement yields functional bias at the human complement receptor, C5aR1. *J Biol Chem* 294: 9416 – 9429

Pandey S, Roy D, Shukla AK (2019b) Measuring surface expression and endocytosis of GPCRs using whole-cell ELISA. *Methods Cell Biol* 149: 131 – 140

Peterson YK, Luttrell LM (2017) The diverse roles of arrestin scaffolds in G protein-coupled receptor signaling. *Pharmacol Rev* 69: 256 – 297

Ranjan R, Dwivedi H, Baidya M, Kumar M, Shukla AK (2017) Novel structural insights into GPCR-beta-arrestin interaction and signaling. *Trends Cell Biol* 27: 851 – 862

Reiter E, Lefkowitz RJ (2006) GRKs and beta-arrestins: roles in receptor silencing, trafficking and signaling. *Trends Endocrinol Metab* 17: 159 – 165

Reiter E, Ahn S, Shukla AK, Lefkowitz RJ (2012) Molecular mechanism of beta-arrestin-biased agonism at seven-transmembrane receptors. *Annu Rev Pharmacol Toxicol* 52: 179 – 197

Ren XR, Reiter E, Ahn S, Kim J, Chen W, Lefkowitz RJ (2005) Different G protein-coupled receptor kinases govern G protein and beta-arrestin-mediated signaling of V2 vasopressin receptor. *Proc Natl Acad Sci USA* 102: 1448 – 1453

Shenoy SK, Lefkowitz RJ (2011) beta-Arrestin-mediated receptor trafficking and signal transduction. *Trends Pharmacol Sci* 32: 521 – 533

Shihoya W, Izume T, Inoue A, Yamashita K, Kadji FMN, Hirata K, Aoki J, Nishizawa T, Nureki O (2018) Crystal structures of human ETB receptor provide mechanistic insight into receptor activation and partial activation. *Nat Commun* 9: 4711

Shukla AK, Violin JD, Whalen EJ, Gesty-Palmer D, Shenoy SK, Lefkowitz RJ (2008) Distinct conformational changes in beta-arrestin report biased agonism at seven-transmembrane receptors. *Proc Natl Acad Sci USA* 105: 9988 – 9993

Shukla AK, Xiao K, Lefkowitz RJ (2011) Emerging paradigms of beta-arrestin-dependent seven transmembrane receptor signaling. *Trends Biochem Sci* 36: 457 – 469

Shukla AK, Manglik A, Kruse AC, Xiao K, Reis RI, Tseng WC, Staus DP, Hilger D, Uysal S, Huang LY, *et al* (2013) Structure of active beta-arrestin-1 bound to a G-protein-coupled receptor phosphopeptide. *Nature* 497: 137 – 141

Shukla AK, Westfield GH, Xiao K, Reis RI, Huang LY, Tripathi-Shukla P, Qian J, Li S, Blanc A, Oleskie AN, *et al* (2014) Visualization of arrestin recruitment by a G-protein-coupled receptor. *Nature* 512: 218 – 222

Simaan M, Bedard-Goulet S, Fessart D, Gratton JP, Laporte SA (2005) Dissociation of beta-arrestin from internalized bradykinin B2 receptor is necessary for receptor recycling and resensitization. *Cell Signal* 17: 1074 – 1083

Srivastava A, Gupta B, Gupta C, Shukla AK (2015) Emerging functional divergence of beta-arrestin isoforms in GPCR function. *Trends Endocrinol Metab* 26: 628 – 642

Staus DP, Hu H, Robertson MJ, Kleinhenz ALW, Wingler LM, Capel WD, Latorraca NR, Lefkowitz RJ, Skiniotis G (2020) Structure of the M2 muscarinic receptor-beta-arrestin complex in a lipid nanodisc. *Nature* 579: 297 – 302

Wei H, Ahn S, Shenoy SK, Karnik SS, Hunyady L, Luttrell LM, Lefkowitz RJ (2003) Independent beta-arrestin 2 and G protein-mediated pathways for angiotensin II activation of extracellular signal-regulated kinases 1 and 2. *Proc Natl Acad Sci USA* 100: 10782 – 10787

Yin W, Li Z, Jin M, Yin YL, de Waal PW, Pal K, Yin Y, Gao X, He Y, Gao J, *et al* (2019) A complex structure of arrestin-2 bound to a G protein-coupled receptor. *Cell Res* 29: 971 – 983

Zhou XE, He Y, de Waal PW, Gao X, Kang Y, Van Eps N, Yin Y, Pal K, Goswami D, White TA, *et al* (2017) Identification of phosphorylation codes for arrestin recruitment by G protein-coupled receptors. *Cell* 170: 457 – 469

Zimmerman B, Simaan M, Akoume MY, Houri N, Chevallier S, Seguela P, Laporte SA (2011) Role of ssarrestins in bradykinin B2 receptor-mediated signalling. *Cell Signal* 23: 648 – 659

Zimmerman B, Beautrait A, Aguila B, Charles R, Escher E, Claing A, Bouvier M, Laporte SA (2012) Differential beta-arrestin-dependent conformational signaling and cellular responses revealed by angiotensin analogs. *Sci Signal* 5: ra33